

AMPA receptors (AMPA-Rs) mediate fast excitatory signaling in the brain, and a change in their number or function underlies lasting forms of synaptic plasticity^{1,2}. At many central synapses the time course of the excitatory postsynaptic current reflects the rapid deactivation of AMPARs following fast neurotransmitter clearance from the cleft^{3–5}. AMPAR desensitization, where the channel closes while glutamate remains bound, is also important in shaping transmission, especially during periods of high-frequency synaptic input⁶ or when glutamate clearance is slow^{7,8}. In this situation, AMPAR-mediated responses are depressed and AMPARs must recover from desensitization before they can be re-activated^{8–10}. Thus, the balance between AMPAR desensitization and recovery influences the amplitude, duration, and frequency of neuronal responses¹¹.

AMPA-Rs are homo- or heterotetrameric assemblies of the pore-forming subunits GluA1–4. The activation, deactivation, and desensitization of the receptor is controlled by ligand-binding domains (LBDs) which form a self-contained clamshell-like structure within each of the four subunits^{12,13}. Glutamate binds between the upper (D1) and lower (D2) lobes of these structures. Within the resting receptor, LBDs of adjacent subunits form dimers that are linked back-to-back between their D1 domains^{12,14}. Following glutamate binding, closure of the LBD clamshell around the agonist causes separation of the D2 domains, applying tension to linkers between the LBDs and the ion channel which opens the gate^{12,15–17}. This can be followed by desensitization, which is initiated by rupturing of the D1–D1 interfaces, relieving the tension on the pore linkers imposed by glutamate binding, allowing the channel to close^{14,16,18,19}.

In neurons, AMPARs are intimately associated with numerous classes of auxiliary subunits, which include the transmembrane AMPAR regulatory proteins (TARPs)²⁰ and germ cell-specific gene 1-like protein (GSG1L)^{21,22}. These auxiliary proteins determine many biophysical and pharmacological properties of AMPARs and influence their desensitization^{23,24}. The prototypical TARP γ -2 markedly slows the rate of AMPAR desensitization and accelerates recovery from desensitization^{25,26}, while TARP γ -8 and GSG1L slow both the entry into and the recovery from desensitization^{21,22,27}. The structures of desensitized complexes, composed of homomeric GluA2 AMPARs with either the prototypical TARP γ -2 or GSG1L, have recently been determined at ~ 8 Å resolution by cryo-electron microscopy (cryo-EM)^{16,19}. The desensitized structures displayed a closed pore, a ruptured D1 interface, and a modest rearrangement (relaxation) of the LBD dimer with closely apposed D2 lobes¹⁸. This contrasts with the more variable LBD structures of GluA2 seen in the absence of auxiliary subunits^{28,29}.

Native GluA2 is subject to RNA editing which causes a switch from the genetically encoded glutamine (Q) to an arginine (R) in the selectivity filter; this Q/R editing reduces channel conductance and Ca^{2+} permeability^{30–32}. Structural details of the closed, desensitized, and activated states of auxiliary subunit-associated homomeric GluA2(R) and GluA2(Q) have been well characterized^{16,17,19,33}. Here we describe striking differences in the functional properties of homomeric GluA2(Q) and GluA2(R) receptors. The edited (R) form displays unusual desensitization and gating behavior when compared with the unedited (Q) form, or indeed any other AMPAR assembly that we have examined^{34–38}. Specifically, we find that GluA2(R) displays a particularly large fractional steady-state current and an anomalous current–variance relationship. When GluA2(R) is expressed with TARPs (γ -2 or γ -8) or with GSG1L we observe similarly anomalous behavior. We suggest that this behavior can be attributed to pore loop arginines preventing desensitization-mediated channel closure of the GluA2(R) assemblies, giving rise to conducting desensitized receptors. Using functional

cysteine cross-linking we exploited this phenomenon to gain insight into the structure of desensitized AMPARs in the plasma membrane.

Results

Atypical channel behavior of Q/R-edited GluA2. When recording glutamate-evoked currents (10 mM, 100 ms, -60 mV) in outside-out patches excised from HEK293 cells expressing homomeric GluA2 with and without γ -2, γ -8, or GSG1L, we observed unexpected differences in the behavior of the unedited (Q) and edited (R) forms (Fig. 1). Compared with that of the Q-forms, GluA2(R) desensitization was slower (Fig. 1a–c). The mean differences in the weighed time constants of desensitization ($\tau_{w, \text{des}}$) between the R- and Q-forms were 4.53 ms (95% confidence interval, 3.71–5.35) for GluA2 alone, 2.13 ms (95% confidence interval, 0.49–3.90) for GluA2/ γ -2, 6.36 ms (95% confidence interval, 2.91–9.65) for GluA2/ γ -8, and 2.83 ms (95% confidence interval, 1.28–4.56) for GluA2/GSG1L. This slowing of desensitization by Q/R site editing was accompanied by a striking increase in fractional steady-state current for GluA2, GluA2/ γ -2, and GluA2/ γ -8 (Fig. 1a, b, d). The mean differences in I_{SS} (% peak) between the R- and Q-forms were 9.2 (95% confidence interval, 6.6–11.1) for GluA2 alone, 33.9 (95% confidence interval, 29.2–38.4) for GluA2/ γ -2, and 24.2 (95% confidence interval, 18.5–30.1) for GluA2/ γ -8. By contrast, I_{SS} was not increased in the case of GluA2/GSG1L (1.43; 95% confidence interval, -0.35 ; 3.25) (Fig. 1d). Of note (except for GluA2/GSG1L) Q/R site editing had a much more pronounced effect on the steady-state currents (~ 400 – 600% increase) than on the desensitization time course (~ 30 – 90% slowing).

In order to determine the underlying weighted mean single-channel conductance for the Q- and R-forms of the receptors we used non-stationary fluctuation analysis (NSFA) (Fig. 1a, b, e). Such analysis typically produces current–variance relationships that can be fitted by a parabolic function which extrapolates to the origin^{36,37}. All GluA2(Q) combinations yielded plots with these features. Consistent with previous reports^{37,38}, the estimated weighted mean single-channel conductance of GluA2(Q) (16.5 ± 1.3 pS, $n = 12$) (mean \pm s.e.m. from n patches) was increased by co-expression with γ -2 or γ -8 (to 32.8 ± 2.0 and 34.6 ± 4.8 pS; $n = 18$ and 7, respectively) but reduced by co-expression with GSG1L (to 11.7 ± 1.0 pS, $n = 6$) (Fig. 1f). The mean differences were 16.3 pS (95% confidence interval, 11.9–20.8), 18.1 pS (95% confidence interval, 10.8–29), and -4.8 pS (95% confidence interval, -7.93 to -2.06). By contrast, NSFA of GluA2(R) receptor combinations produced anomalous current–variance relationships that were right-shifted (Fig. 1b, e), precluding conventional interpretation. This shift, which was apparent for GluA2(R) alone, was accentuated by expression with TARPs γ -2 or γ -8, but was reduced by co-expression of GSG1L (Fig. 1e). Such current–variance relationships have not been reported for other AMPAR complexes^{34–38}.

To determine the basis of the anomalous results from NSFA, we focused on GluA2(R)/ γ -2, which displayed the most robust expression, the greatest increase in steady-state current, and the most right-shifted current–variance relationship. First, we observed a near identical current–variance relationship for the tandem construct GluA2(R) $_{\gamma$ -2 (Supplementary Fig. 1a). This suggests that the anomalous behavior of co-expressed GluA2(R) and γ -2 did not simply reflect the presence of AMPARs with different TARP stoichiometries, and thus heterogeneous channel properties³⁹. Second, shifted relationships were also seen with GluA2(R)/ γ -2 at $+60$ mV (Supplementary Fig. 1b, c). As channels would be passing Cs^+ rather than Na^+ in this condition, this argues that the phenomenon is independent of both voltage and permeating ion. Third, we obtained anomalous current–variance

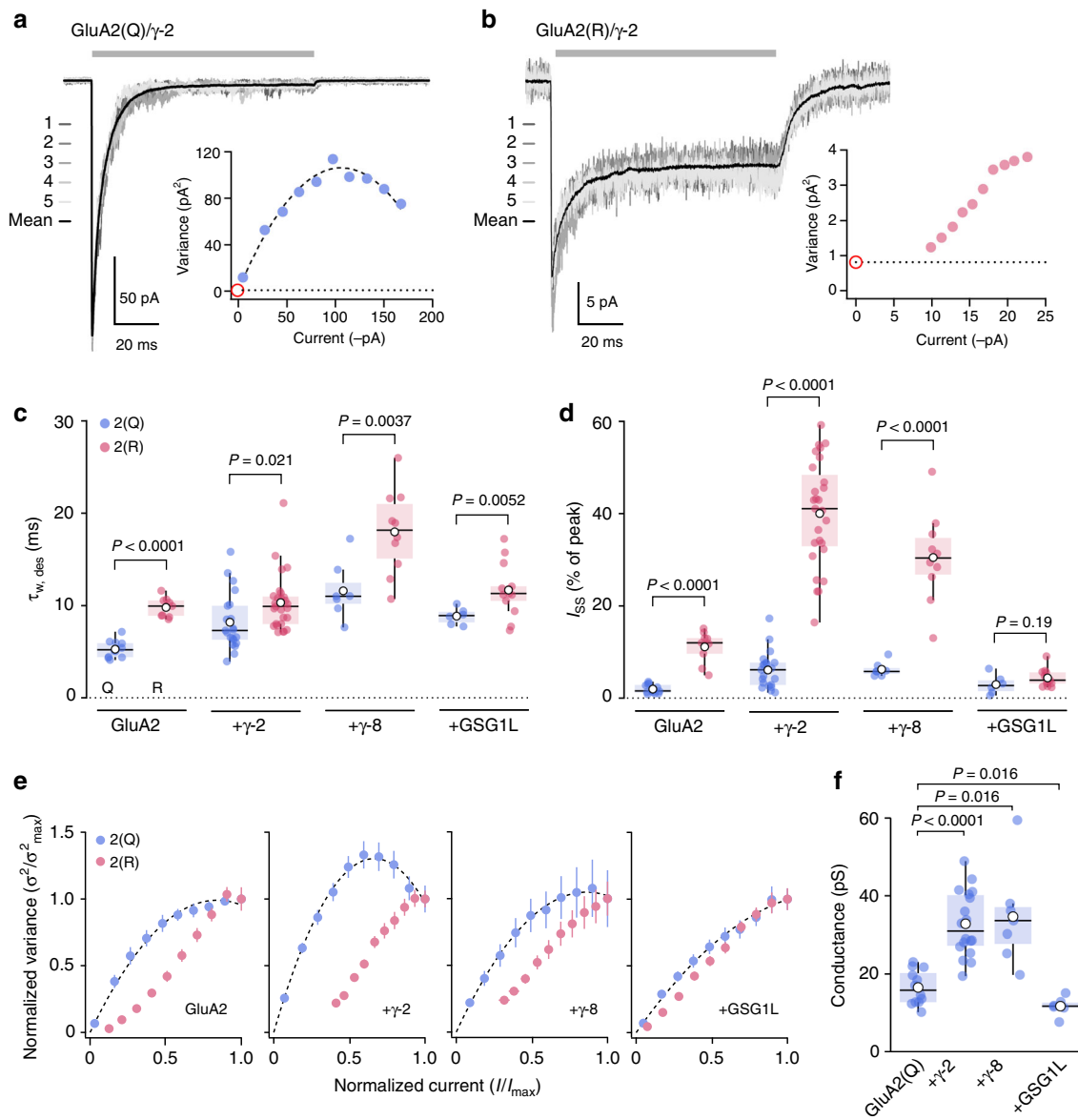


Fig. 1 Q/R editing affects the kinetics and variance of GluA2 currents. **a** Representative outside-out patch response (10 mM glutamate, 100 ms, -60 mV; gray bar) from a HEK293 cell transfected with GluA2(Q)/ γ -2 (average current, black; five individual responses, grays). Inset: current-variance relationship (dotted line indicates background variance and red circle indicates expected origin). **b** As **a**, but for GluA2(R)/ γ -2. Note that the data cannot be fitted with a parabolic relationship passing through the origin. **c** Pooled $\tau_{w,des}$ data for GluA2 alone ($n = 12$ Q-form and 9 R-form), GluA2/ γ -2 ($n = 21$ and 27), GluA2/ γ -8 ($n = 7$ and 10), and GluA2/GSG1L ($n = 6$ and 13). Box-and-whisker plots indicate the median (black line), the 25-75th percentiles (box), and the 10-90th percentiles (whiskers); filled circles are data from individual patches and open circles indicate means. Two-way ANOVA revealed an effect of Q/R editing ($F_{1,97} = 111.34$, $P < 0.0001$), an effect of auxiliary subunit type ($F_{3,97} = 32.3$, $P < 0.0001$) and an interaction ($F_{3,97} = 2.84$, $P = 0.041$). **d** Pooled data for I_{ss} . Box-and-whisker plots and n numbers as in **c**. Two-way ANOVA indicated an effect of Q/R editing ($F_{1,97} = 129.98$, $P < 0.0001$), an effect of auxiliary subunit type ($F_{3,97} = 58.30$, $P < 0.0001$), and an interaction ($F_{3,97} = 58.67$, $P < 0.0001$). **e** Doubly normalized and averaged current-variance relationships (desensitizing current phase only) from GluA2(Q) and GluA2(R) expressed alone ($n = 12$ and 9), with γ -2 ($n = 19$ and 23), with γ -8 ($n = 7$ and 10), or with GSG1L ($n = 6$ and 13). Error bars are s.e.m.s. All Q-forms can be fitted with parabolic relationships passing through the origin, while R-forms cannot. **f** Pooled NSFA conductance estimates for GluA2(Q) alone, GluA2(Q)/ γ -2, GluA2(Q)/ γ -8, and GluA2(Q)/GSG1L ($n = 12$, 18, 7, and 6, respectively). Box-and-whisker plots as in **c**. Indicated P values are from Wilcoxon rank sum tests. Source data are provided as a Source Data file

relationships with the edited form of GluA4 (GluA4(R)/ γ -2) (Supplementary Fig. 1d), indicating that the behavior is not confined to GluA2(R) receptors. Fourth, current-variance relationships derived from deactivation of GluA2(R)/ γ -2 (following 1 or 100 ms glutamate exposure; Supplementary Fig. 2a-e) and from GluA2(R)/ γ -2 or GluA4(R)/ γ -2 (following 1 ms glutamate exposure; Supplementary Fig. 2f, g) also displayed non-parabolic features. Taken together, our results reveal that the

behavior of homomeric Q/R-edited AMPARs deviates substantially from that expected.

GluA2(R)/ γ -2 receptors display two types of channel opening. Stationary fluctuation analysis of GluA2(R) currents in the absence of TARPs has previously yielded an estimated conductance of ~ 300 fS³². While single-channel openings of this

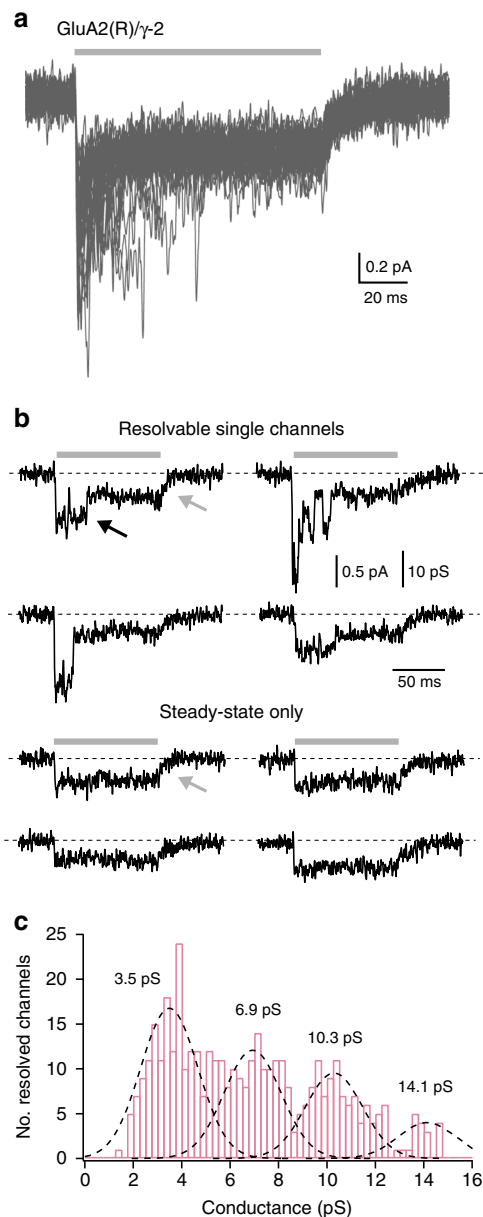


Fig. 2 GluA2(R)/ γ -2 single-channel recordings. **a** GluA2(R)/ γ -2 currents from an outside-out patch containing few channels (-60 mV). Forty consecutive applications of 10 mM glutamate (gray bar) are overlaid. **b** Individual responses exhibiting discrete channel openings superimposed on a persistent steady-state current (upper sweeps) or exhibiting only a persistent steady-state component (lower sweeps). Note the decay of the steady-state currents on glutamate removal (gray arrows) is much slower than the closure of resolved channels (black arrow). **c** Histogram of channel conductance for 392 discernible openings from six patches. The histogram is fit with the sum of four Gaussian curves (dashed lines) with a common standard deviation (1.2 pS), revealing four peaks (3.5 , 6.9 , 10.3 , and 14.1 pS)

magnitude would be too small to resolve directly, in some of our GluA2(R)/ γ -2 patches containing small numbers of channels, we were able to observe discrete single-channel openings that were in the picosiemens range (Fig. 2a, b). A histogram of channel amplitudes (pooled from six patches) revealed that openings to a conductance level of 3.5 pS were the most prevalent (Fig. 2c). The additional peaks above 3.5 pS could reflect either the presence of multiple conductance states, as reported for unedited AMPAR combinations^{26,32,40–42}, or multiple concurrent events.

The resolved openings showed several unusual features. First, despite the steady-state macroscopic current being relatively large ($\sim 40\%$ of the peak current; Fig. 1d), the majority of resolvable individual openings were present at the onset of the glutamate application (Fig. 2a, b). Second, while the amplitudes of resolved openings were equivalent to (or larger than) the steady-state current, the recordings contained no sojourns to the baseline; the resolvable openings thus appeared to ride on a low-noise background current (Fig. 2a, b). Third, throughout the recordings, occasional responses were observed in which the current onset showed no discernible picosiemens openings. Nonetheless, these responses still exhibited the low-noise steady-state current (Fig. 2b). Fourth, unlike the rapid closure of the resolved picosiemens channel openings, the steady-state current decay that followed agonist removal was slow (and roughly exponential), as might be expected if it reflected the closure of a large number of lower conductance openings (Fig. 2b). These results suggest that GluA2(R)/ γ -2 receptors are capable of generating two distinct types of channel opening—conventional AMPAR openings (with conductances in the picosiemens range) which form the initial phase of the macroscopic response, along with openings of much lower conductance that form the steady-state current. The pattern of channel behavior we observed—predominantly large openings occurring at the onset of the response and predominantly small openings at steady-state—would give rise to a steady-state current with relatively low variance, consistent with the right-shifted current–variance relationships (Fig. 1e).

GluA2(R) receptors in the absence of auxiliary subunits exhibit detectable chloride permeability (P_{Cl}/P_{Cs} estimated as 0.14 , ref. ⁴³). We asked whether the different classes of channel openings seen with GluA2(R)/ γ -2 could have different relative chloride permeabilities. To address this, we applied 100 ms pulses of glutamate and measured the reversal potential of the peak and steady-state currents (comprising mostly large and small openings, respectively) in external solutions containing high (145 mM) or low (35 mM) CsCl⁴³ (Supplementary Fig. 3). The expected shift in reversal potential following a switch between these conditions is -30.4 mV for a Cs⁺-selective (Cl⁻ impermeable) channel and $+30.1$ mV for a purely Cl⁻-selective channel (see Methods). We recorded shifts in reversal potential of -36.0 ± 1.4 and -33.7 ± 2.1 mV for the peak and steady-state currents, respectively ($n = 7$, $P = 0.100$; Supplementary Fig. 3), suggesting that the different classes of channel opening do not differ in their relative chloride permeability. Indeed, this result suggests that in the presence of γ -2, GluA2(R) receptors mediate negligible Cl⁻ flux.

Low conductance steady-state openings follow desensitization.

NSFA for both desensitization and deactivation gave current–variance relationships that were not amenable to conventional interpretation. We thus sought to determine whether NSFA of the rising phase of the current (AMPA activation) could accurately report weighted mean single-channel conductance and, if so, whether this approach might be applicable to GluA2(R)/ γ -2. We first confirmed that NSFA of the fast-rising AMPAR activation phase would allow us to estimate accurately the single-channel conductance of unedited GluA2(Q)/ γ -2. This yielded a weighted mean conductance of 24.7 ± 4.3 pS, not different from that obtained from the analysis of deactivating current (26.4 ± 3.1 pS; $P = 0.64$, paired t -test, $n = 5$; Fig. 3a, b). For GluA2(R)/ γ -2 activation (unlike the deactivation phase of the same records) we obtained conventional parabolic current–variance relationships yielding a weighted mean conductance of 3.8 ± 0.5 pS ($n = 10$; Fig. 3c, d), similar to the most prevalent conductance seen in our single-channel analysis (Fig. 2c).

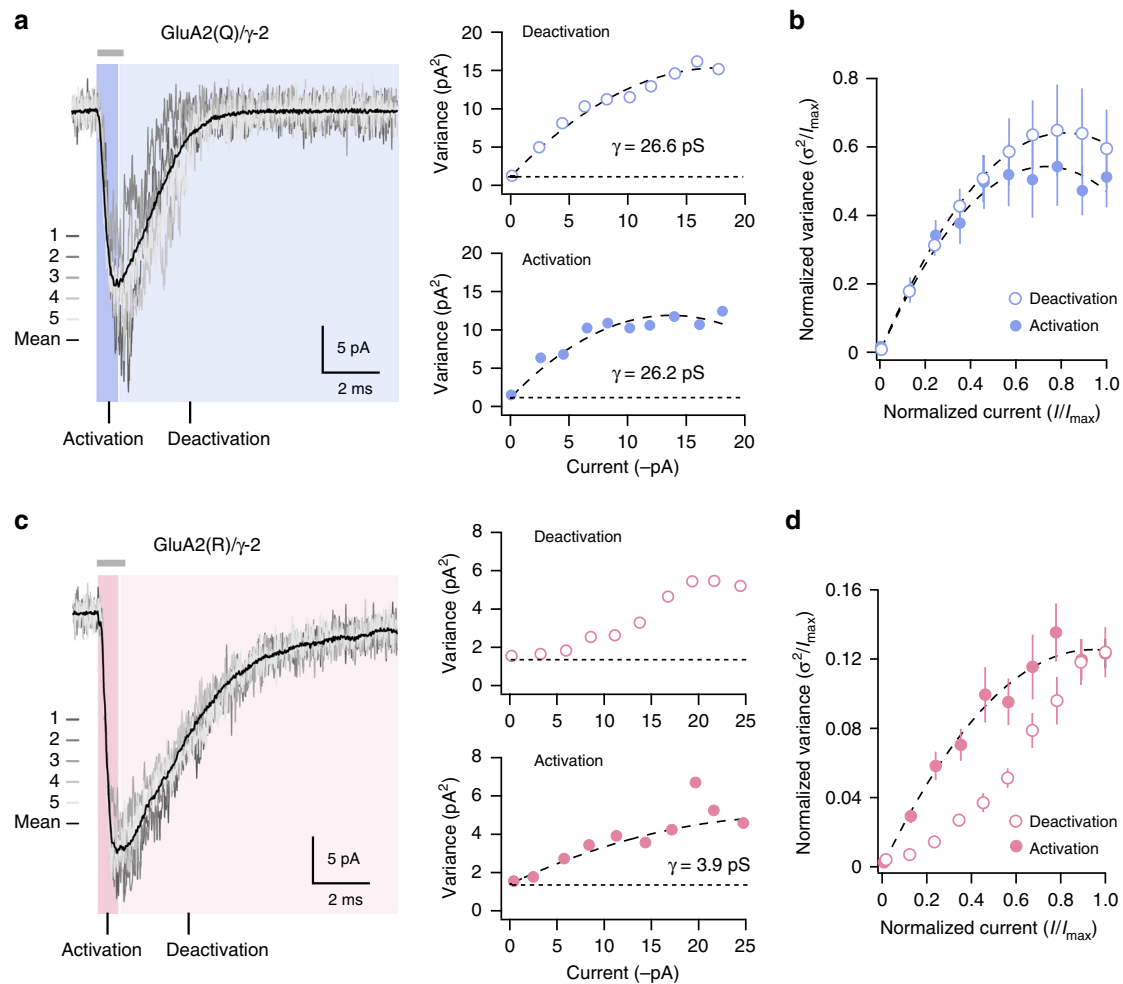


Fig. 3 Estimated weighted mean conductance from NSFA of GluA2(R)/ γ -2 activation. **a** Representative GluA2(Q)/ γ -2 responses to 1 ms (gray bar) glutamate application (gray traces) with superimposed average (black trace). NSFA was performed on the activation phase (blue highlight; filled blue circles) and deactivation phase (light blue highlight; open blue circles) of the same records, yielding similar estimates of weighted mean conductance. **b** Pooled current-variance plots for the activation and deactivation of GluA2(Q)/ γ -2 currents ($n = 5$). Error bars indicate s.e.m. **c** Representative GluA2(R)/ γ -2 response to 1 ms glutamate application (as in **a**). NSFA was performed on the activation phase (pink highlight; filled pink circles) and deactivation phase (light pink highlight; open pink circles) of the same records. Current-variance relationship is non-parabolic for deactivation but parabolic for activation. **d** Pooled current-variance plots for the activation and deactivation of GluA2(R)/ γ -2 currents ($n = 8$). Error bars indicate s.e.m.

As conventional current-variance relationships could be produced only from GluA2(R)/ γ -2 activation and not desensitization (nor indeed from deactivation, during which there is a degree of desensitization) we speculated that desensitization itself may provide the key to our unexpected results. We hypothesized that the conformational rearrangements of the LBDs which normally trigger desensitization might not fully close the ion channel, such that the GluA2(R)/ γ -2 receptors could adopt a conducting desensitized state, giving rise to the large fractional steady-state current and the anomalous current-variance relationships. If this were the case, and the shift from large resolvable channel openings to smaller openings was linked to the process of desensitization, a decline in GluA2(R)/ γ -2 single-channel conductance (and therefore macroscopic current) would not be expected if desensitization was blocked. In the presence of cyclothiazide, which inhibits desensitization by stabilizing the upper LBD dimer interface¹⁴, we found that GluA2(R)/ γ -2 macroscopic currents (10 mM glutamate, 1 s) did not decay (Fig. 4a). Likewise, if the low-noise steady-state current of GluA2(R)/ γ -2 arose from conducting desensitized channels, then we would expect the steady-state current to remain when desensitization was enhanced. To test this idea, we used the point

mutation S754D. This weakens the upper LBD dimer interface, accelerating desensitization and reducing steady-state currents of GluA2(Q)¹⁴. For both GluA2(Q)/ γ -2 and GluA2(R)/ γ -2 the S754D mutation produced a near 20-fold acceleration of desensitization (Fig. 4b, c) and a greater than twofold slowing of recovery from desensitization (Fig. 4d). As anticipated, GluA2(Q) S754D/ γ -2 produced a negligible steady-state current (Fig. 4b, e). In marked contrast, GluA2(R) S754D/ γ -2 exhibited an appreciable steady-state current (Fig. 4b, e). The presence of a large steady-state current with GluA2(R)/ γ -2 under conditions strongly favoring desensitization is consistent with the view that desensitized channels can conduct.

A model incorporating conducting desensitized receptors. We next considered whether the presence of desensitized receptors able to conduct ions could account quantitatively for our observations. To examine this, we incorporated such states into a modified version of a kinetic scheme we used previously to describe AMPAR/TARP concentration-dependent behaviors^{25,44} (Scheme 1; Fig. 5a), and attempted to mimic the macroscopic kinetics and NSFA of GluA2(R)/ γ -2 by varying the rate constants and conductances. From six patches in which activation,

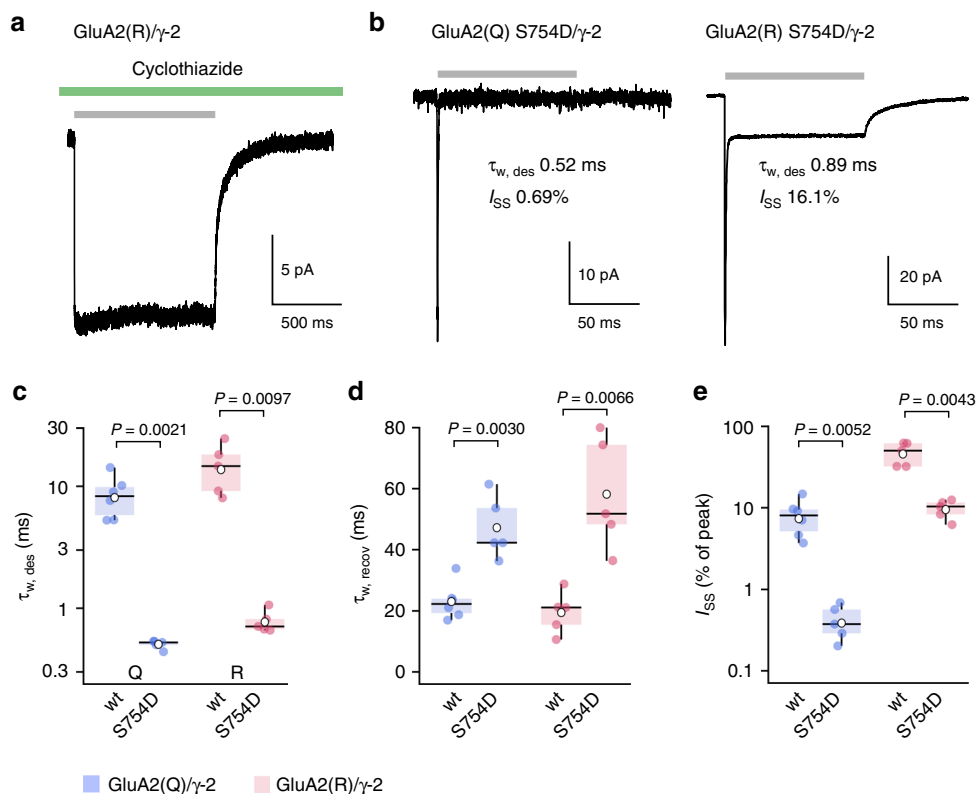


Fig. 4 Large steady-state GluA2(R)/ γ -2 currents are observed even in conditions favoring desensitization. **a** Representative GluA2(R)/ γ -2 current (-60 mV) evoked by 10 mM glutamate (gray bar) in the presence of 50 μ M cyclothiazide (green bar). Note the minimal current decay when desensitization is inhibited (for pooled data $I_{SS}/I_{peak} = 93.4 \pm 1.6\%$, $n = 6$) (mean \pm s.e.m. from n patches). **b** Representative glutamate-evoked currents from Q- and R-forms of GluA2 S754D/ γ -2. Both forms exhibit very fast desensitization, but the R-form has an appreciable steady-state current. **c** Pooled data showing desensitization kinetics ($\tau_{w,des}$) for wild-type (wt; $n = 6$ and 5) and mutant (S754D; $n = 5$ and 5) forms of GluA2(Q)/ γ -2 and GluA2(R)/ γ -2. Box-and-whisker plots as in Fig. 1c. Two-way ANOVA indicated an effect of Q/R editing ($F_{1,17} = 10.56$, $P = 0.0047$), an effect of the mutation ($F_{1,17} = 43.19$, $P < 0.0001$) but no interaction ($F_{1,17} = 2.63$, $P = 0.12$). The mean difference between S754D and wild type was -8.1 ms (95% confidence interval, -10.9 to -6.0) for Q and -14.1 ms (95% confidence interval, -20.0 to -9.3) for R. **d** Pooled data (as in **c**) for recovery kinetics ($\tau_{w,recov}$). Two-way ANOVA indicated no effect of Q/R editing ($F_{1,17} = 0.13$, $P = 0.72$), an effect of the mutation ($F_{1,17} = 31.67$, $P < 0.0001$) but no interaction ($F_{1,17} = 1.65$, $P = 0.22$). The mean difference between S754D and wild type was 24.1 ms (95% confidence interval, 15.3 to 33.2) for Q and 38.7 ms (95% confidence interval, 23.7 to 53.9) for R. **e** Pooled data (as in **c**) for the fractional steady-state current (I_{SS}). Two-way ANOVA indicated an effect of Q/R editing ($F_{1,17} = 65.37$, $P < 0.0001$), an effect of the mutation ($F_{1,17} = 28.37$, $P < 0.0001$) and an interaction ($F_{1,17} = 14.93$, $P = 0.0012$). The mean difference in I_{SS} (% of peak) between S754D and wild type was -7.7 (95% confidence interval, -11.2 to -5.2) for Q and -37.9 (95% confidence interval, -49.2 to -25.8) for R. Indicated P values are from Welch t -tests. Source data are provided as a Source Data file

deactivation, and desensitization were all examined, we generated global average waveforms and current–variance plots for each condition (Fig. 5b–d). The inclusion in our scheme of conducting desensitized states allowed simultaneous modeling of all kinetic and current–variance data.

The model yielded estimated conductances of 3.9 pS for the fully open state and 670 fS for the fully occupied desensitized state of GluA2(R)/ γ -2. As the steady-state occupancy of desensitized receptors (D1*–D4*, D22*–D24* combined: 90%) was much higher than that of the open receptors (O1–O4 combined: 6%), the latter contributed just 27% of the steady-state current. The low conductance and high steady-state occupancy of desensitized channels predicted by the model can fully explain the unusually low variance of the large steady-state current and, therefore, the right-shifted current–variance relationship produced from the macroscopic desensitizing current (Fig. 1). The model indicated that the proportion of current carried by desensitized and non-saturated receptors increased during deactivation (from 11% and 6%, respectively, at the peak, to 25% and 77% at mid-decay). The combination of these factors could explain the rapid fall-off in deactivation variance (Supplementary Fig. 2). While alternative

kinetic schemes remain possible (see Supplementary Discussion), we favor Scheme 1 as the simplest that can account for our experimental findings with homomeric GluA2(R) complexes.

Functional cross-linking of desensitized receptors. Recent work on the structural basis of desensitization has shown that the variety of conformations adopted by the desensitized LBD layer is greatly diminished when the full-length AMPAR is co-assembled with auxiliary subunits^{16,19,28,29}. In the presence of γ -2 the LBD dimers of desensitized GluA2 favor a relaxed dimer conformation, with the upper D1–D1 interfaces ruptured and the lower D2 domains more closely apposed, allowing channel closure¹⁶. We reasoned that conducting desensitized receptors could enable us to determine whether this conformation (previously revealed through crystallography and cryo-EM) can indeed be adopted by AMPARs in the plasma membrane. Specifically, we predicted that if the steady-state current of GluA2(R) reflected ion flow through desensitized receptors in the relaxed dimer conformation, then if trapped in this conformation the receptors should maintain their

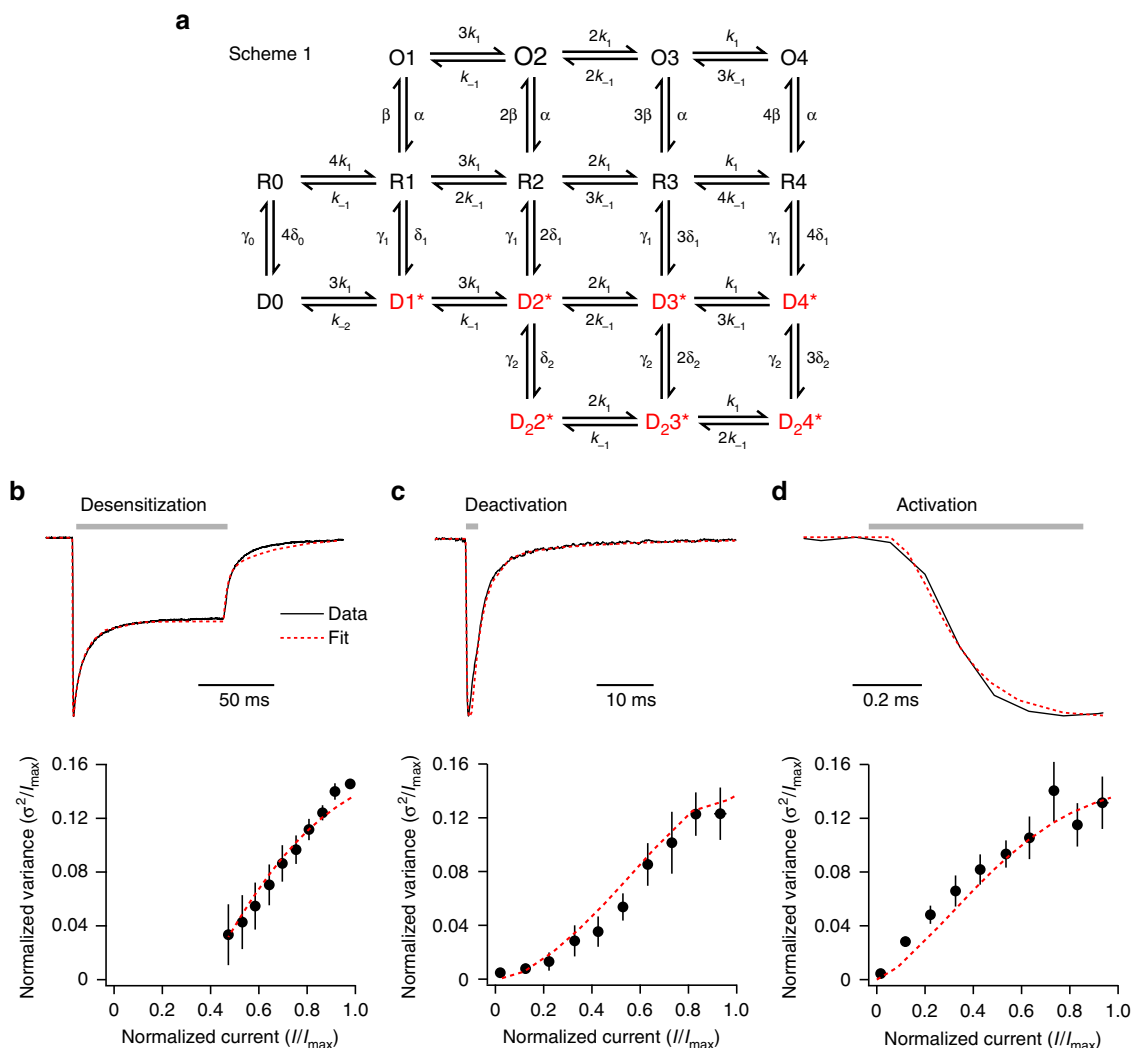


Fig. 5 A kinetic scheme including conducting desensitized states can mimic GluA2(R)/ γ -2 behavior. **a** Scheme 1 is a modified form of a previously proposed kinetic model^{25,44}. States which can conduct are red. Open states (O1–O4) and occupied desensitized states (D1*–D4*, D₂2*–D₂4*) have independent conductances that are occupancy-dependent. **b–d** Global averaged GluA2(R)/ γ -2 records (top) and variance data (bottom) for desensitization, deactivation, and activation (10 mM glutamate—gray bars). Using a single set of rate constants and conductances, the model closely mimics all six measures (dashed red lines): $k_1 = 1.3 \times 10^6 \text{ M}^{-1} \text{ s}^{-1}$, $k_{-1} = 350 \text{ s}^{-1}$, $\alpha = 3100 \text{ s}^{-1}$, $\beta = 1000 \text{ s}^{-1}$, $\gamma_1 = 88 \text{ s}^{-1}$, $\delta_1 = 110 \text{ s}^{-1}$, $\gamma_2 = 36 \text{ s}^{-1}$, $\delta_2 = 39 \text{ s}^{-1}$, $\gamma_0 = 8 \text{ s}^{-1}$, $\delta_0 = 0.48 \text{ s}^{-1}$, $k_{-2} = 870 \text{ s}^{-1}$, conductance of fully occupied open state (O4) = 3.9 pS, conductance of fully occupied desensitized state (D4* and D₂4*) = 670 fS. Conductances of partially occupied states were proportional to their occupancy (e.g. O3 = 0.75 × O4, O2 = 0.5 × O4, O1 = 0.25 × O4)

conductance. To test this, we introduced cysteines at sites on the central axis of the D2–D2 dimer interface, cross-linking of which has previously been shown to inhibit channel opening by trapping the receptor in desensitized-like states. Thus we compared S729C, cross-linking of which permits the relaxed dimer conformation^{16,18,45}, with G724C⁴⁶ which we predicted would not accommodate the relaxed dimer conformation when cross-linked (Supplementary Fig. 4). In each case, we examined the effect of cross-linking on GluA2 currents.

We first simulated currents from wild-type GluA2(R)/ γ -2 receptors (Scheme 1), and compared these with simulated currents expected from receptors occupying only desensitized states (Scheme 2; Fig. 6a, b). These simulations predicted that if cross-linking trapped receptors in the native conducting desensitized state, it would change the glutamate response to a purely non-decaying steady-state current of reduced size.

To investigate the functional effects of cysteine cross-linking, and test these predictions, we examined the sensitivity of both unedited and edited GluA2 G724C/ γ -2 and S729C/ γ -2 receptors

to the oxidizing agent CuPhen⁴⁵. Application of CuPhen to both editing forms of GluA2 G724C/ γ -2 receptors caused rapid inhibition of glutamate-evoked currents, resembling the reported effects of cross-linking on TARP-free receptors⁴⁶ (Fig. 6c; Supplementary Fig. 5a). The peak and steady-state currents generated by GluA2(Q) S729C/ γ -2 were also inhibited by CuPhen (Fig. 6d; Supplementary Fig. 5b). By contrast, cross-linking of edited GluA2(R) S729C/ γ -2 abolished the peak current, but not the steady-state current (Fig. 6d; Supplementary Fig. 5b)—a result consistent with the predictions of Scheme 2. Similar results were also seen when GluA2(R) S729C was expressed with γ -8 or GSG1L (Supplementary Fig. 5c). Overall, these results demonstrate that ion permeation through desensitized channels allows possible LBD conformations of the desensitized wild-type receptor to be probed using functional cross-linking. Of the two LBD conformations we examined, only S729C, which can accommodate the relaxed dimer state when cross-linked, behaved in a manner resembling that of the wild-type desensitized channel.

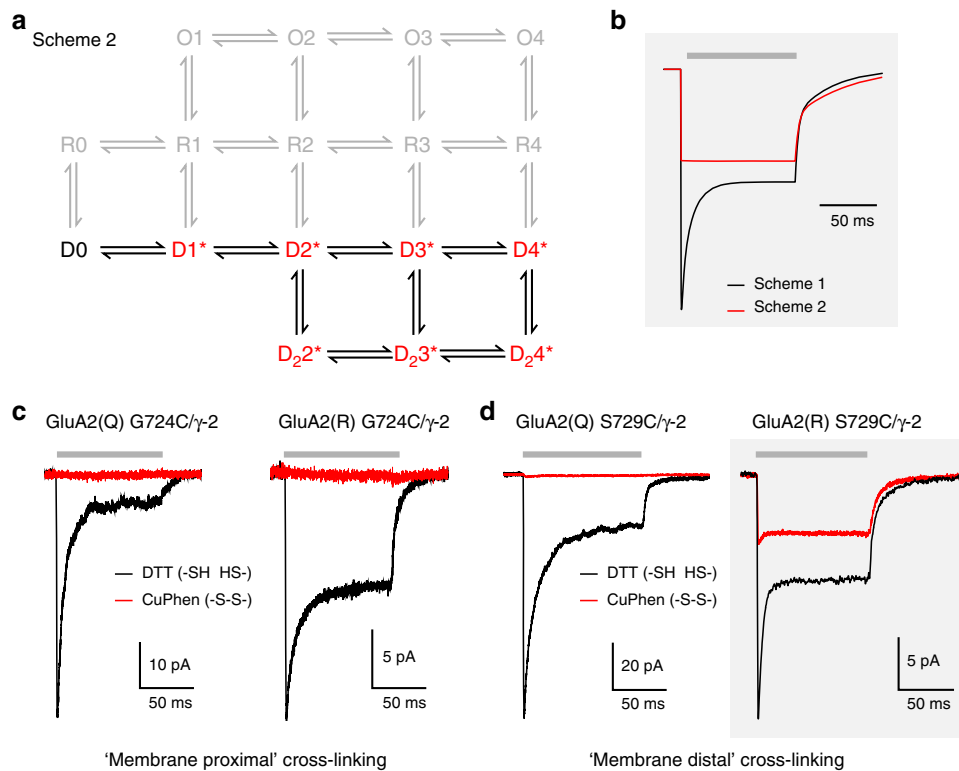


Fig. 6 A model with access to only desensitized states predicts behavior of cross-linked GluA2(R) S729C/γ-2. **a** Scheme 2 is modified from Scheme 1 (Fig. 5a) and assumes that, following cross-linking, the receptor can occupy only desensitized states (excluded states are shown in gray). **b** Simulated responses to 10 mM glutamate (gray bar) using Scheme 1 to mimic the non-cross-linked condition and Scheme 2 to mimic the effect of cross-linking. **c** Representative currents at -60 mV activated by 10 mM glutamate (gray bar) from GluA2(Q) G724C/γ-2 and GluA2(R) G724C/γ-2 in DTT (black) or CuPhen (red). Note that, for both forms, currents are fully inhibited following cross-linking by 10 μM CuPhen. **d** Representative responses from individual patches demonstrate that following cross-linking by 10 μM CuPhen, GluA2(Q) S729C/γ-2 currents are inhibited, while GluA2(R) S729C/γ-2 currents show minimal desensitization and continue to display a large steady-state current, as predicted in **a**. Gray boxes (**b** and **d**) highlight the similarity of modeled currents and recorded GluA2(R) S729C/γ-2 currents

Antagonist-bound cross-linked GluA2 LBD structures. Our functional data demonstrate that cross-linked GluA2(R) S729C/γ-2 receptors retain sensitivity to glutamate, implying that upon agonist binding they can undergo structural change which affects the channel gate. To understand the molecular basis of this, we determined the crystal structure of cross-linked S729C ligand binding cores in apo-like conformations bound to the competitive antagonists NBQX (diffracted to 1.8 Å resolution) or ZK200775 (diffracted to 2.0 Å) (Fig. 7a; Supplementary Fig. 6). AMPAR gating is driven by the separation of the D2-M3 linker regions following agonist binding^{12,16,17}. Thus, binding of glutamate is known to increase the distance between the α-carbons of Proline 632 pairs at the base of the D2 lobe of the GluA2 LBD (Fig. 7a)^{12,15,47}. For the cross-linked S729C mutant LBD bound with NBQX (S729C_{NBQX}) the Proline 632 separation was 22.8 Å (similar to that seen with S729C_{ZK}, 22.6 Å). This is less than the separation we calculate for the glutamate-bound mutant LBD (S729C_{glu}, 26.4 Å)¹⁸. The relative separation of Pro632 residues suggests that, despite being constrained by the cross-link, glutamate binding to GluA2(R) S729C can trigger relative movements of the lower LBDs which, in the intact receptor, may induce tension in the M3-D2 linkers sufficient to allow ion flow (Fig. 7b).

We also crystallized isolated cross-linked G724C LBDs in both the apo-like ZK200775-bound form (G724C_{ZK}) and desensitized-like glutamate-bound forms in two different space groups (G724C_{glu} Forms A and B; Supplementary Fig. 7). As we anticipated, G724C_{ZK} demonstrated reduced Pro632 separation (19.2 Å) compared to the antagonist-bound S729C forms, in

keeping with the greater constraints on LBD separation imposed by G724C. However, unlike glutamate-bound S729C^{18,45}, neither form of G724C_{glu} adopted a relaxed dimer conformation (Fig. 7b). Instead they displayed a non-biological conformation, with a large rotation and total loss of the dimer interface which cannot be accommodated within the intact receptor (Supplementary Fig. 7). Thus, the Pro632 separation in the intact, cross-linked GluA2 G724C receptor could not be meaningfully assessed.

Discussion

Our experimental findings have implications for the understanding of AMPAR desensitization. They challenge the idea that the pore of desensitized AMPARs must be fully closed, and provide direct functional evidence concerning the conformation of the LBDs of desensitized receptors. Our NSFA, single-channel measurements and kinetic modeling all support the unexpected conclusion that atypical currents generated by GluA2(R)/γ-2 arise from desensitized receptors that retain around one-sixth of the maximal conductance of open channels. Our data indicate a weak, previously unidentified, coupling between the desensitized LBD and the gate, that is revealed only in Q/R-edited homomers, and is strengthened by TARP association. While a conducting desensitized state has previously been described for a mutant, homomeric, α7 nicotinic acetylcholine receptor⁴⁸, to our knowledge such behavior for a ligand-gated ion channel formed from wild-type subunits has not previously been described. The presence of a conducting desensitized state of GluA2(R) provided us with a functional readout to probe the likely arrangement of

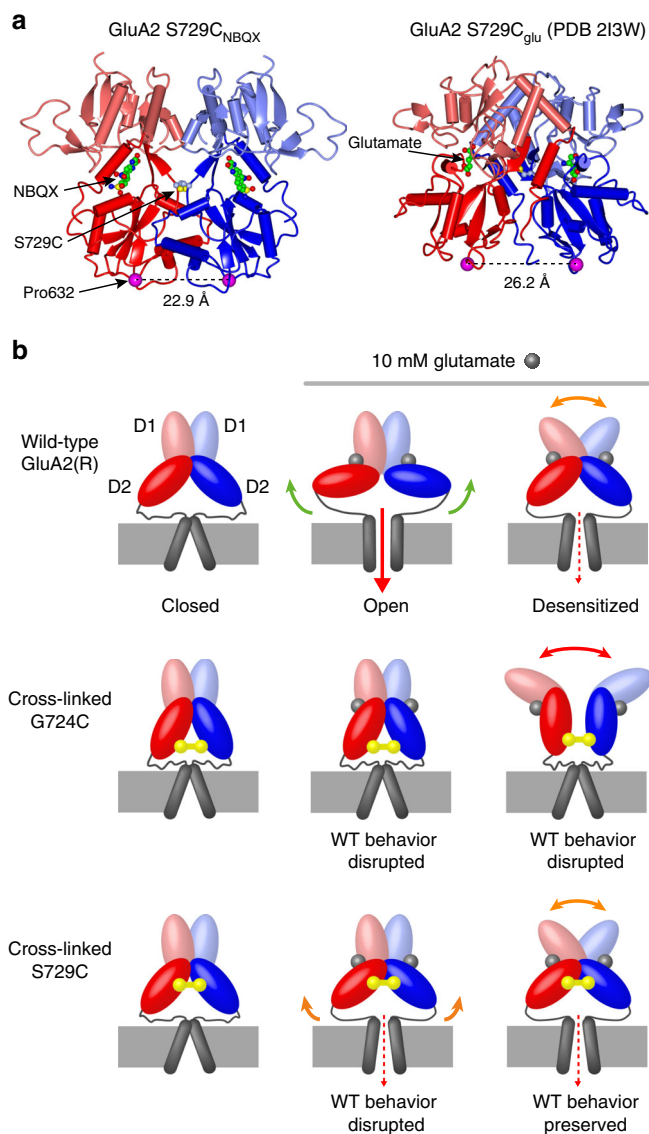


Fig. 7 Cross-linked S729C LBD structures suggest a model of gating for desensitized GluA2(R). **a** Left, crystal structure of the dimeric GluA2 S729C ligand-binding core in the presence of NBQX, with the upper (D1, pale) and lower (D2, dark) lobes of each monomer (red and blue) distinguished by shading. The structure is viewed perpendicular to the axis between the C α atoms of Pro632 (magenta spheres). Right, crystal structure of the GluA2 S729C ligand-binding core in the presence of glutamate (S729C_{glu}; PDB: 2I3W)¹⁸. The Pro632 separation seen in the presence of glutamate (right) is >3 Å greater than that seen with NBQX (left). **b** Cartoon representing possible conformations of the GluA2(R) LBD dimer and pore in our functional cross-linking recordings. Non-cross-linked GluA2(R) channels bind glutamate (gray spheres), closing the clamshell LBDs and opening the pore to the full open channel conductance. Desensitization does not fully close the pore. As determined in the presence of γ -2, cross-linking of the G724C mutant (yellow) does not allow the action of agonist binding to be communicated to the pore in any state, and disrupts the normal dimeric conformation of desensitized receptors. Cross-linking of the S729C mutant (yellow) is not compatible with the full open state, but the channel can adopt the normal desensitized conformation, meaning that (as with the non-cross-linked receptor) the pore is not closed

LBDs within desensitized AMPARs. By comparing currents from GluA2(R)/ γ -2, GluA2(R)/ γ -8, and GluA2(R)/GSG1L receptors with those from constrained cross-linked cysteine mutants^{18,46}, we have established that the relaxed dimer conformation identified in structural studies¹⁸ is indeed representative of desensitized AMPARs within the plasma membrane.

What is the evidence that the steady-state current does indeed arise from desensitized AMPARs? The fractional steady-state glutamate-evoked currents we recorded with GluA2(R)/ γ -2 were much larger than those of other AMPAR/auxiliary subunit combinations we have examined previously^{34–38}. While one might reasonably suppose that such a large steady-state current could arise simply from a reduced level of receptor desensitization, a number of the GluA2(R)/ γ -2 properties we have identified suggest this is not the case. Importantly, the rates of entry into, and recovery from, desensitization for GluA2(R)/ γ -2 were similar to those for GluA2(Q)/ γ -2, which had a much smaller steady-state current. Moreover, a reduced extent of desensitization would not give rise to the rightward shift in the current–variance relationships that we observed. By contrast, the presence of a substantial steady-state current of unusually low variance would produce such a shift. Thus, the steady-state current could be generated by low-conductance channels with a high open probability. Furthermore, resolvable (pico Siemens) openings were common at the onset of the current, but occurred only rarely during steady-state, supporting the view that these contribute little to the large steady-state component. Finally, AMPAR mutations (S754D and S729C) that enhanced desensitization essentially eliminated steady-state currents of GluA2(Q)/ γ -2 receptors, but had much less effect on steady-state currents of GluA2(R)/ γ -2 receptors. Consequently, our data suggest that a large fraction of the GluA2(R)/ γ -2 steady-state current arises from conducting desensitized channels.

How do our functional data fit with recently published AMPAR structures? Cryo-EM analysis has indicated that the pore diameter at the M3 gate of agonist-bound desensitized GluA2(R)/ γ -2 is less than that of the activated receptor¹⁶ and similar to that of the closed (antagonist-bound) receptor³³. Thus, the occurrence of conducting desensitized states could be seen to present something of a paradox. The single closed structure for desensitized GluA2(R)/ γ -2 (ref. 16) indicates that open desensitized states were not present under the conditions used for cryo-EM analysis or, if present, were either too heterogeneous to allow reconstruction, or perhaps too similar in structure to closed desensitized states to be classified distinctly. At the same time, although our kinetic and current–variance data could be adequately mimicked by Scheme 1 without the inclusion of closed desensitized receptors, our data do not preclude their existence. For simplicity, we assigned a conductance to all occupied desensitized states, but models including both closed and conducting desensitized states could also broadly reproduce our functional data. Nonetheless, the magnitude of the steady-state current (relative to the peak current) limits how many closed desensitized channels are likely to be present in our recordings. Of note, rapid transitions between these states would be required to account for the absence of clear channel closures from steady state in our single-channel records. Taken together, it is certainly possible that both closed and open desensitized receptors are present in cryo-EM conditions, in which closed desensitized channels might predominate, as well as in our recordings, in which conducting desensitized channels are clearly prevalent.

In our model of GluA2(R)/ γ -2 gating, assigning fully occupied desensitized channels a conductance of 670 fS provided a good approximation to both our kinetic and noise data. While currents mediated by GluA2(R), GluA2(R)/ γ -8, and GluA2(R)/GSG1L also bore all the hallmarks of conducting desensitized channels,

for these combinations the deviations from conventional parabolic current–variance relationships were less dramatic, and the editing-dependent increases in steady-state current were smaller. Furthermore, when co-expressed with γ -8 or GSG1L, cross-linking of the GluA2(R) S729C mutant displayed a smaller residual steady-state current than that seen when it was co-expressed with γ -2. One possible explanation for these differences is that for GluA2(R) receptors the rank-order of desensitized channel conductance is γ -2 > γ -8 > no auxiliary > GSG1L. An alternative possibility is that this reflects the presence of both conducting and non-conducting desensitized states. In this latter scenario, our macroscopic data could be explained by γ -2-associated receptors spending a greater proportion of time than GluA2(R), GluA2(R)/ γ -8, or GluA2(R)/GSG1L in conducting desensitized states, relative to closed desensitized states.

Recently, a chimeric AMPAR/KAR construct (ATD and LBD of GluK2 with TM and C-tail of GluA2) has been shown to exhibit a large leak current when co-expressed with TARPs⁴⁹. Remarkably, when these chimera/TARP combinations were exposed to glutamate the currents decreased, suggesting that, despite conducting in the absence of agonist, desensitization could still cause closure of the channel⁴⁹. The existence of a leak current in the presence of a TARP was taken to indicate that TARPs disrupt the ligand-free closed state of the receptor, leading to spontaneous channel opening. Although we found no evidence that edited GluA2 receptors open spontaneously when expressed with a TARP, the existence of receptors that conduct when desensitized—and the fact that the magnitude of the steady-state current is greatest when γ -2 is present—supports the view that TARPs can also disrupt channel closure in the desensitized state, in a manner that is Q/R-editing-dependent.

How might Q/R site editing render the desensitized GluA2 receptor ion permeable? Of note, in the case of the homologous Q/R-edited kainate receptor GluK2(R), the homomeric receptors are markedly more sensitive to block by *cis*-unsaturated fatty acids than are GluK2(R)/K1(Q) heteromers⁵⁰. Structural modeling of the pore loop arginines of the GluK2(R) homomers suggests their side chains project away from the cytoplasm and towards the gate, and the resultant interaction between the pore loop and the M3 helix proximal to the gate is proposed to influence fatty acid pharmacology⁵¹. While the orientation of the arginine side chains in the desensitized state has yet to be resolved, in the activated structure of the GluA2(R)/ γ -2 receptor¹⁶ (and in closed heteromeric GluA1/2(R) $_{\gamma}$ -8; ref. ²⁷) they too project away from the cytoplasm and towards the gate. If such interactions are present in desensitized GluA2(R)/ γ -2, these might modify the rearrangement of the channel gate following desensitization, thereby hampering full channel closure. Alternatively, given structural evidence that the Q/R site may act as an additional gate of the receptor¹⁷, charge–charge repulsion between arginines at this site might specifically compromise the constriction at this gate, which may be sufficient, on its own, to account for the ion flow through desensitized channels.

There is general agreement that desensitization-induced AMPAR pore closure is caused by LBD rearrangements which allow the base of the D2 lobes to assume positions similar to those of the apo/inactivated form, thereby releasing the tension exerted by the M3-S2 linkers on the M3 helix caused by glutamate binding^{16,19}. In the absence of auxiliary proteins there is considerable heterogeneity in the LBD and ATD layers of desensitized AMPARs^{28,29}. However, when associated with γ -2 or GSG1L, AMPAR LBD dimers show increased stability of a single relaxed dimer conformation^{16,18,19}. The fact that GluA2(R) S729C, co-expressed with auxiliary subunits and trapped in the relaxed dimer conformation by cross-linking, exhibited properties consistent with those of wild-type channels, demonstrates that

this conformation does indeed mimic the behavior of the native desensitized receptor in the plasma membrane. By contrast, functional cross-linking of a different mutant GluA2(R) G724C/ γ -2—which did not assume a relaxed LBD dimer when crystallized—trapped these receptors in a non-conducting state, indicating that this conformation must be distinct from that of native desensitized AMPARs. It is noteworthy that despite the constraint on LBD movement imposed by cross-linking at S729C, the current produced by cross-linked GluA2(R)/ γ -2 was glutamate-dependent, suggesting agonist binding produces changes within the constrained LBD layer sufficient to influence the pore. Dimeric Pro632 separation within S729C ligand-binding core crystals in the presence of glutamate¹⁸ is greater than the separation we observed in the presence of competitive antagonists. While this suggests that glutamate binding might exert only a small degree of tension on the LBD-TM linkers within the cross-linked receptors, in the intact receptor (especially in the presence of TARPs that prevent loss of tension due to LBD compression towards the transmembrane domains^{16,19}), this might be sufficient to open the gate. However, the Pro632 measure provides only a one-dimensional approximation of a complex three-dimensional process. Future cryo-EM analysis of full-length GluA2 S729C may provide valuable further information on the complex dynamics of desensitized receptors.

Do conducting desensitized states of homomeric GluA2(R) contribute to neuronal or glial signaling? Neurons and glia normally express multiple AMPAR subunit isoforms. When GluA2 is co-expressed with other subunits (in the absence of auxiliary proteins) the formation of GluA2 homomers is strongly discriminated against, in favor of GluA2-containing heteromers^{52,53}. Nonetheless, trafficking of homomeric GluA2(R) is enhanced if the receptors are unedited at the secondary (R/G) editing site⁵⁴, and we (and others^{55,56}) have demonstrated that the presence of γ -2 allows robust heterologous expression of functional GluA2(R) homomers. Of note, glutamate-gated channels with femtomens conductance have been detected in cerebellar granule cells⁵⁷. Moreover, an immunoprecipitation study that suggested hippocampal AMPARs were predominantly GluA1/2 or GluA2/3 heteromers did not expressly rule out the presence of GluA2 homomers^{58,59}. Additionally, functional GluA2(R) homomers can be trafficked to hippocampal synapses by endogenous TARPs following the conditional deletion of the alleles for GluA1 and GluA3 (ref. ⁶⁰). Whether, in the presence of multiple GluA subtypes, TARPs facilitate the formation of GluA2(R) homomers remains to be determined. Nevertheless, it is clear from recent cryo-EM analysis of native AMPARs that homomeric GluA2 receptors exist in the brain⁶¹, and our findings suggest that they can conduct even when desensitized.

Methods

Heterologous expression. We expressed recombinant AMPAR subunits and TARPs (plus EGFP) in HEK293 cells (a gift from Trevor Smart, UCL). These were maintained under standard protocols, as described previously²⁵. AMPAR subunit cDNAs (rat) were flip splice variants and the GluA2 forms were additionally R/G edited. Point mutations of the GluA2 subunit were produced using standard PCR protocols. Primer sequences are listed in Supplementary Table 1. AMPAR/TARP combinations were transfected at a cDNA ratio of 1:2. The GluA2 $_{\gamma}$ -2 tandem consisted of full-length GluA2 and a nine amino-acid linker (GGGGGFAT) before the start codon of full-length γ -2. Transient transfection was performed using Lipofectamine 2000 (Life Technologies). Cells were split 12–30 h after transfection and plated on glass coverslips in the presence of 50 μ M NBQX (2,3-dioxo-6-nitro-1,2,3,4-tetrahydrobenzo[*f*]quinoxaline-7-sulfonamide; Tocris-Abcam) to avoid AMPAR-mediated toxicity. Electrophysiological recordings were performed 18–48 h later.

Electrophysiology. Patch-clamp electrodes were pulled from borosilicate glass (1.5 mm o.d., 0.86 mm i.d.; Harvard Apparatus) and fire polished to a final resistance of 8–12 M Ω . For outside-out patches the external solution contained 145 mM NaCl, 2.5 mM KCl, 1 mM CaCl₂, 1 mM MgCl₂, and 10 mM HEPES, pH 7.3.

The internal solution contained 145 mM CsCl, 2.5 mM NaCl, 1 mM Cs-EGTA, 4 mM MgATP, and 10 mM HEPES (pH 7.3 with CsOH) supplemented with 100 μ M spermine tetrahydrochloride (Tocris Bioscience). Currents with a risetime >500 μ s were rejected. For chloride permeability experiments, two CsCl based solutions were used—one with high CsCl (145 mM CsCl, 10 mM HEPES, 1 mM CaCl₂, pH 7.3 with CsOH) and one with low CsCl (CsCl reduced to 35 mM and osmolarity adjusted with glucose). For recordings involving cysteine cross-linking, control and agonist solutions were supplemented with 1 mM DTT to reduce disulfide bonds or 10 μ M CuCl and 30 μ M 1–10-phenanthroline (CuPhen) to promote disulfide formation⁴⁵. The effects of CuPhen were fully reversible by 1 mM DTT. Recordings were made from outside-out patches at 22–25 °C using an Axopatch 200A amplifier (Molecular Devices). Currents were recorded at –60 mV, low-pass filtered at 10 kHz, and digitized at 20 kHz, except for recordings to assess activation noise which were digitized at 100 kHz (Digidata 1440A interface with pClamp 10 software; Molecular Devices). Patches with small responses were filtered at 2 kHz to more readily identify single-channel openings, and digitized at 10 kHz.

Rapid agonist application to excised patches. Rapid agonist application was achieved by switching between continuously flowing solutions. Solution exchange was achieved by moving an application tool made from theta glass (Hilgenberg; 2 mm outer diameter, pulled to a tip opening of ~200 μ m) mounted on a piezo-electric translator (Physik Instrumente). At the end of each experiment, the adequacy of the solution exchange was tested by destroying the patch and measuring the liquid-junction current at the open pipette (10–90% rise time typically 150–250 μ s).

Data analysis. Entry into desensitization (100 ms application of 10 mM glutamate) and current deactivation (1 ms) were fitted with the sum of two exponentials using IGOR Pro 6.35 (Wavemetrics) with NeuroMatic⁶² and the weighted time constant (τ_w) calculated. Recovery from steady-state desensitization was measured following a 100 ms equilibrating application of 10 mM glutamate. The recovery of glutamate-activated peak currents was measured following 2–200 ms intervals in control solution.

Records used for single-channel analysis were filtered at 0.5 kHz and individual channel events were selected by eye. Channel openings were analyzed using QuB (ver. 2.0.0.7; <https://qub.mandelics.com>). The amplitude of the resolved openings was measured from the closing transition (final current level to steady-state current). Measured openings (at –60 mV) were binned by conductance and fitted using a multi-peak Gaussian function (IGOR Pro).

NSFA was performed on the decaying phase of currents evoked by 1 or 100 ms applications of 10 mM glutamate (35–300 successive applications), as previously described³⁶. The variance for each successive pair of current responses was calculated and the single-channel current (i) and total number of channels (N) were then determined by plotting the ensemble variance (σ^2) against mean current (\bar{I}) and fitting with a parabolic function:

$$\sigma^2 = i\bar{I} - \bar{I}^2/N + \sigma_B^2, \quad (1)$$

where σ_B^2 is the background variance⁶³. For NSFA of current activation, records were digitized at a high sampling rate (100 kHz) to ensure sufficient numbers of data points from the average record could be grouped into each of the ten amplitude bins. As alignment of traces on their rising phases (as used for deactivation and desensitization records) led to a distortion of activation noise, analysis was instead performed on unaligned traces (from sections of recording in which the time of the current onset was stable; Spearman Stability Analysis, NeuroMatic).

Experimentally determined shifts in reversal potentials following local exchange from the high to low CsCl solutions were compared to the calculated shifts (for purely Cs⁺-permeable and purely Cl⁻-permeable channels) determined using the equation:

$$V_{\text{rev}} = \frac{RT}{F} \ln \frac{a\text{Cs}_o + (P_{\text{Cl}}/P_{\text{Cs}})a\text{Cl}_i}{a\text{Cs}_i + (P_{\text{Cl}}/P_{\text{Cs}})a\text{Cl}_o}, \quad (2)$$

where V_{rev} is the reversal potential measured at the peak or steady-state, $P_{\text{Cl}}/P_{\text{Cs}}$ is the permeability ratio of chloride relative to cesium and $a\text{Cs}$ and $a\text{Cl}$ are the activities of the ions in the intracellular (i) and extracellular (o) solutions⁴³. F , R , and T have their usual meanings. $a\text{Cs}$ in the high CsCl solution was extrapolated from tabulated values to be 0.714 (https://web.archive.org/web/20190228144112/http://www.kayelab.npl.co.uk/chemistry/3_9/3_9_6.html). $a\text{Cs}$ in the low CsCl solution was estimated to be 0.824. This value has a small degree of uncertainty, as the effect of glucose—demonstrated to modestly affect $a\text{Na}$ in NaCl solutions⁶⁴—is unknown. Our chosen value assumes a similar effect of glucose on the activities of both NaCl and CsCl. Seals were formed and patches obtained in the standard NaCl external solution. The two experimental CsCl solutions were applied locally (interleaved) while the bath was continuously perfused with standard external. No correction was applied for liquid-junction potentials.

Kinetic modeling. Kinetic simulations and fits were performed in Scilab 5.5.0. (Scilab Enterprises; <https://www.scilab.org>) using the Q-matrix method⁶⁵. Rate constants were adapted from our previous model for GluA1/ γ -2 (refs. 25,26). For

each iteration of the rate constants, currents were calculated from the occupancies of all conducting states at given time points multiplied by their unitary current. Noise was calculated using the following equation:⁶⁶

$$\sigma^2 = i^2 N p(1-p), \quad (3)$$

where N is the number of channels of unitary current i of open probability p . The ensemble variance for a channel with multiple subconductances was calculated as the sum of the variances for each state:

$$\sigma^2 = N \sum_{j=1}^k (i_j^2 p_j (1-p_j)), \quad (4)$$

where k is the number of conducting states, j refers to each conducting state, and i_j and p_j are its unitary current and occupancy respectively. N was re-derived from the experimentally measured peak current as well as the peak open probability and conductance of each state for each iteration of the fit. Kinetics and noise of desensitization, deactivation, and activation, across six patches from which all properties could be measured, were normalized, averaged, and fit using Scheme 1 (Fig. 5). Kinetic data were parsed (to 35 data points) to make computation manageable. While all variables contributed to the model output, certain rates were strongly influenced by particular aspects of the data: k_1 —activation kinetics; k_{-1} —deactivation kinetics; α , β —activation kinetics, steady-state current, and current–variance relationships; γ_1 , δ_1 , γ_2 , and δ_2 —desensitization kinetics and steady-state current; γ_0 , δ_0 —current–variance relationships and desensitization; open channel conductance—all current–variance relationships; desensitized conductance—current–variance relationship of desensitization. Rate constant k_{-2} was constrained by microscopic reversibility.

Expression and purification of ligand-binding cores. Cysteine mutants of the GluA2 flop S1S2-binding core with an N-terminal octahistidine tag in the pET22b vector¹² were produced using standard PCR protocol (see Supplementary Table 1). Following transformation of Origami B cells (VWR; 71408–3), high levels of protein were expressed by induction with 0.5 mM IPTG when the cells had reached OD₆₀₀ ~1.2. The cells were harvested by centrifugation following overnight incubation at 20 °C. Harvested cells were washed once with PBS and resuspended in HisTrap binding buffer (50 mM Tris, pH 8; 150 mM NaCl; 20 mM imidazole; protease inhibitor cocktail (Roche), and 50 μ M NBQX to displace glutamate and promote dimerization). Resuspended cells were treated with lysozyme for 30 min at 4 °C and cell membranes were disrupted by sonication and removed by centrifugation. Samples were filtered (0.45 μ m) to remove residual cellular debris and loaded onto a HisTrap Column (GE Healthcare) at 4 °C. Protein was eluted using HisTrap elution buffer (50 mM Tris pH 8; 150 mM NaCl; 300 mM imidazole) and aliquots containing the highest concentrations of dimers were pooled for further purification. Parallel reducing and non-reducing SDS-PAGE and Coomassie blue staining established that ligand-binding cores preferentially formed cross-linked dimers with no need for exogenous oxidation. Protein was concentrated using 10 kDa concentrators before exchanging into column buffer (50 mM Tris, pH 8; 150 mM NaCl). Histidine tags were cleaved using thrombin. A final purification step (in column buffer) was performed with a size exclusion column (Superdex 200; GE Healthcare, Little Chalfont, UK). Final purified AMPAR LBDs were concentrated to 2–7 mg ml⁻¹.

Protein crystallography. Crystallization was achieved using sitting drop vapor diffusion at 16 °C. All crystals appeared within 72 h, and were harvested after 1–2 weeks. For each crystal, precipitant solutions, and additives for cryoprotection prior to freezing, differed. GluA2 S729C_{NBQX}: 0.1 M tri-sodium citrate pH 5.5, 20% PEG 3000. Supplemented with 15% glycerol for cryoprotection. GluA2 S729C_{ZK}/GluA2 G724C_{ZK}: 0.2 M ammonium chloride, 20% PEG 3350, 10 μ M ZK200775. Supplemented with 15% glycerol for cryoprotection. GluA2 G724C_{glu} Form A: 1 M lithium chloride, 0.1 M citric acid pH 4.0, 20% (w/v) PEG 6000, 30 mM glutamate. Supplemented with 20% glycerol for cryoprotection. GluA2 G724C_{glu} Form B: 0.16 M calcium acetate, 0.08 M sodium cacodylate pH 6.5, 14.4% (w/v) PEG 8000, 20% (v/v) glycerol, 1 mM glutamate. No additives necessary for cryoprotection.

Diffraction data were collected at Diamond Light Source beamlines I04 and I24, and at ESRF ID30B (see Supplementary Table 2). Diffraction data were initially processed using Xia2 (ref. 67) and AIMLESS⁶⁸. Initial molecular replacement was performed using Phaser⁶⁹ and structures were refined using PHENIX⁷⁰ and Coot⁷¹. Structures G724C_{ZK}, S729C_{NBQX}, and S729C_{ZK} were solved using the ZK200775-bound wild-type LBD (PDB 3KGC)¹³ as the search model. Both forms of G724C_{glu} were solved using the glutamate-bound wild-type LBD (PDB 1FTJ)¹² as the search model. Cysteines were modeled into cryo-EM structures of GluA2(R)/ γ -2 in the activated and desensitized forms using PyMOL (The PyMOL Molecular Graphics System, Version 2.0 Schrödinger, LLC), and the separation of the sulfur atoms was determined. The separation of Ca Pro632 atoms in LBD structures was also measured using PyMOL.

Data presentation and statistical analysis. Summary data are presented in the text as mean \pm s.e.m. (from n patches). Comparisons involving two data sets only were performed using a paired t -test or unpaired Welch two-sample t -test that does not assume equal variance (normality was not tested statistically, but gauged from

quantile–quantile (Q–Q) plots and/or density histograms). Comparisons of multiple conditions were performed using two-sided Welch two-sample *t*-tests with Holm’s sequential Bonferroni correction. When comparing Q and R edited forms of AMPARs, analyses were performed using two-way analysis of variance (Welch heteroscedastic *F*-test) followed by pairwise comparisons using two-sided Welch two-sample *t*-tests. Exact *P* values are presented to two significant figures, except when *P* < 0.0001. Statistical tests were performed using R (version 3.3.3, the R Foundation for Statistical Computing, <https://www.r-project.org/>) and R Studio (version 1.1.383, RStudio). Independent-samples confidence intervals for the differences between two population means were obtained using a bias-corrected and accelerated (BCa) bootstrap method in R⁷². No statistical test was used to pre-determine sample sizes; these were based on standards of the field. No randomization was used. A full list of statistical analyses is provided in Supplementary Table 3.

Reporting summary. Further information on research design is available in the Nature Research Reporting Summary linked to this article.

Data availability

Data supporting the findings of this manuscript are available from the corresponding authors upon reasonable request. The data underlying Fig. 1c, d, f, 4c–e and Supplementary Figs 1c and 2b are provided as a Source Data file. The coordinate and structure factor data for the GluA2 LBD crystals have been deposited in the Protein Data Bank (PDB) with the following accession codes: S729C_{NBQX}, 6FQH; S729C_{ZK}, 6FQK; G724C_{ZK}, 6FQJ; G724C_{glu} Form A, 6FQG; G724C_{glu} Form B, 6FQL.

Code availability

Computer code demonstrating example calculations for the current and non-stationary fluctuation analysis presented in Fig. 5 is available from the UCL Research Data Repository: <https://doi.org/10.5522/04/8797892>.

Received: 22 March 2019 Accepted: 28 August 2019

Published online: 20 September 2019

References

- Henley, J. M. & Wilkinson, K. A. Synaptic AMPA receptor composition in development, plasticity and disease. *Nat. Rev. Neurosci.* **17**, 337–350 (2016).
- Huganir, R. L. & Nicoll, R. A. AMPARs and synaptic plasticity: the last 25 years. *Neuron* **80**, 704–717 (2013).
- Cathala, L., Holderith, N. B., Nusser, Z., DiGregorio, D. A. & Cull-Candy, S. G. Changes in synaptic structure underlie the developmental speeding of AMPA receptor-mediated EPSCs. *Nat. Neurosci.* **8**, 1310–1318 (2005).
- Colquhoun, D., Jonas, P. & Sakmann, B. Action of brief pulses of glutamate on AMPA/kainate receptors in patches from different neurones of rat hippocampal slices. *J. Physiol.* **458**, 261–287 (1992).
- Hestrin, S. Activation and desensitization of glutamate-activated channels mediating fast excitatory synaptic currents in the visual cortex. *Neuron* **9**, 991–999 (1992).
- Trussell, L. O., Zhang, S. & Raman, I. M. Desensitization of AMPA receptors upon multiquantal neurotransmitter release. *Neuron* **10**, 1185–1196 (1993).
- Kinney, G. A., Overstreet, L. S. & Slater, N. T. Prolonged physiological entrapment of glutamate in the synaptic cleft of cerebellar unipolar brush cells. *J. Neurophysiol.* **78**, 1320–1333 (1997).
- Otis, T., Zhang, S. & Trussell, L. O. Direct measurement of AMPA receptor desensitization induced by glutamatergic synaptic transmission. *J. Neurosci.* **16**, 7496–7504 (1996).
- Lu, H. W., Balmer, T. S., Romero, G. E. & Trussell, L. O. Slow AMPAR synaptic transmission is determined by stargazin and glutamate transporters. *Neuron* **96**, 73–80 (2017).
- Zampini, V. et al. Mechanisms and functional roles of glutamatergic synapse diversity in a cerebellar circuit. *Elife* **5**, e15872 (2016).
- Jones, M. V. & Westbrook, G. L. The impact of receptor desensitization on fast synaptic transmission. *Trends Neurosci.* **19**, 96–101 (1996).
- Armstrong, N. & Gouaux, E. Mechanisms for activation and antagonism of an AMPA-sensitive glutamate receptor: crystal structures of the GluR2 ligand binding core. *Neuron* **28**, 165–181 (2000).
- Sobolevsky, A. I., Rosconi, M. P. & Gouaux, E. X-ray structure, symmetry and mechanism of an AMPA-subtype glutamate receptor. *Nature* **462**, 745–756 (2009).
- Sun, Y. et al. Mechanism of glutamate receptor desensitization. *Nature* **417**, 245–253 (2002).
- Jin, R., Banke, T. G., Mayer, M. L., Traynelis, S. F. & Gouaux, E. Structural basis for partial agonist action at ionotropic glutamate receptors. *Nat. Neurosci.* **6**, 803–810 (2003).
- Chen, S. et al. Activation and desensitization mechanism of AMPA receptor-TARP complex by cryo-EM. *Cell* **170**, 1234–1246 (2017).
- Twomey, E. C., Yelshanskaya, M. V., Grassucci, R. A., Frank, J. & Sobolevsky, A. I. Channel opening and gating mechanism in AMPA-subtype glutamate receptors. *Nature* **549**, 60–65 (2017).
- Armstrong, N., Jasti, J., Beich-Frandsen, M. & Gouaux, E. Measurement of conformational changes accompanying desensitization in an ionotropic glutamate receptor. *Cell* **127**, 85–97 (2006).
- Twomey, E. C., Yelshanskaya, M. V., Grassucci, R. A., Frank, J. & Sobolevsky, A. I. Structural bases of desensitization in AMPA receptor-auxiliary subunit complexes. *Neuron* **94**, 569–580 (2017).
- Tomita, S. et al. Functional studies and distribution define a family of transmembrane AMPA receptor regulatory proteins. *J. Cell Biol.* **161**, 805–816 (2003).
- Schwenk, J. et al. High-resolution proteomics unravel architecture and molecular diversity of native AMPA receptor complexes. *Neuron* **74**, 621–633 (2012).
- Shanks, N. F. et al. Differences in AMPA and kainate receptor interactomes facilitate identification of AMPA receptor auxiliary subunit GSG1L. *Cell Rep.* **1**, 590–598 (2012).
- Greger, I. H., Watson, J. F. & Cull-Candy, S. G. Structural and functional architecture of AMPA-type glutamate receptors and their auxiliary proteins. *Neuron* **94**, 713–730 (2017).
- Eibl, C. & Pledest, A. J. R. AMPA receptors: mechanisms of auxiliary protein action. *Curr. Opin. Physiol.* **2**, 84–91 (2018).
- Coombs, I. D., MacLean, D. M., Jayaraman, V., Farrant, M. & Cull-Candy, S. G. Dual effects of TARP γ -2 on glutamate efficacy can account for AMPA receptor autoinactivation. *Cell Rep.* **20**, 1123–1135 (2017).
- Tomita, S. et al. Stargazin modulates AMPA receptor gating and trafficking by distinct domains. *Nature* **435**, 1052–1058 (2005).
- Herguedas, B. et al. Architecture of the heteromeric GluA1/2 AMPA receptor in complex with the auxiliary subunit TARP γ 8. *Science* **364**, eaav9011 (2019).
- Durr, K. L. et al. Structure and dynamics of AMPA receptor GluA2 in resting, pre-open, and desensitized states. *Cell* **158**, 778–792 (2014).
- Meyerson, J. R. et al. Structural mechanism of glutamate receptor activation and desensitization. *Nature* **514**, 328–334 (2014).
- Sommer, B., Kohler, M., Sprengel, R. & Seeburg, P. H. RNA editing in brain controls a determinant of ion flow in glutamate-gated channels. *Cell* **67**, 11–19 (1991).
- Burnashev, N., Monyer, H., Seeburg, P. H. & Sakmann, B. Divalent ion permeability of AMPA receptor channels is dominated by the edited form of a single subunit. *Neuron* **8**, 189–198 (1992).
- Swanson, G. T., Kamboj, S. K. & Cull-Candy, S. G. Single-channel properties of recombinant AMPA receptors depend on RNA editing, splice variation, and subunit composition. *J. Neurosci.* **17**, 58–69 (1997).
- Zhao, Y., Chen, S., Yoshioka, C., Bacongus, I. & Gouaux, E. Architecture of fully occupied GluA2 AMPA receptor-TARP complex elucidated by cryo-EM. *Nature* **536**, 108–111 (2016).
- Coombs, I. D. et al. Cornichons modify channel properties of recombinant and glial AMPA receptors. *J. Neurosci.* **32**, 9796–9804 (2012).
- Soto, D., Coombs, I. D., Gratacos-Batlle, E., Farrant, M. & Cull-Candy, S. G. Molecular mechanisms contributing to TARP regulation of channel conductance and polyamine block of calcium-permeable AMPA receptors. *J. Neurosci.* **34**, 11673–11683 (2014).
- Soto, D., Coombs, I. D., Kelly, L., Farrant, M. & Cull-Candy, S. G. Stargazin attenuates intracellular polyamine block of calcium-permeable AMPA receptors. *Nat. Neurosci.* **10**, 1260–1267 (2007).
- Soto, D. et al. Selective regulation of long-form calcium-permeable AMPA receptors by an atypical TARP, γ -5. *Nat. Neurosci.* **12**, 277–285 (2009).
- McGee, T. P., Bats, C., Farrant, M. & Cull-Candy, S. G. Auxiliary subunit GSG1L acts to suppress calcium-permeable AMPA receptor function. *J. Neurosci.* **35**, 16171–16179 (2015).
- Shi, Y., Lu, W., Milstein, A. D. & Nicoll, R. A. The stoichiometry of AMPA receptors and TARPs varies by neuronal cell type. *Neuron* **62**, 633–640 (2009).
- Prieto, M. L. & Wollmuth, L. P. Gating modes in AMPA receptors. *J. Neurosci.* **30**, 4449–4459 (2010).
- Shelley, C., Farrant, M. & Cull-Candy, S. G. TARP-associated AMPA receptors display an increased maximum channel conductance and multiple kinetically distinct open states. *J. Physiol.* **590**, 5723–5738 (2012).
- Zhang, W., Devi, S. P., Tomita, S. & Howe, J. R. Auxiliary proteins promote modal gating of AMPA- and kainate-type glutamate receptors. *Eur. J. Neurosci.* **39**, 1138–1147 (2014).
- Burnashev, N., Villarroel, A. & Sakmann, B. Dimensions and ion selectivity of recombinant AMPA and kainate receptor channels and their dependence on Q/R site residues. *J. Physiol.* **496**, 165–173 (1996).
- Robert, A. & Howe, J. R. How AMPA receptor desensitization depends on receptor occupancy. *J. Neurosci.* **23**, 847–858 (2003).

45. Pledsted, A. J. & Mayer, M. L. AMPA receptor ligand binding domain mobility revealed by functional cross linking. *J. Neurosci.* **29**, 11912–11923 (2009).
46. Yelshanskaya, M. V., Li, M. & Sobolevsky, A. I. Structure of an agonist-bound ionotropic glutamate receptor. *Science* **345**, 1070–1074 (2014).
47. Menuz, K., Stroud, R. M., Nicoll, R. A. & Hays, F. A. TARP auxiliary subunits switch AMPA receptor antagonists into partial agonists. *Science* **318**, 815–817 (2007).
48. Revah, F. et al. Mutations in the channel domain alter desensitization of a neuronal nicotinic receptor. *Nature* **353**, 846–849 (1991).
49. Ben-Yaacov, A. et al. Molecular mechanism of AMPA receptor modulation by TARP/stargazin. *Neuron* **93**, 1126–1137 (2017).
50. Wilding, T. J., Zhou, Y. & Huettner, J. E. Q/R site editing controls kainate receptor inhibition by membrane fatty acids. *J. Neurosci.* **25**, 9470–9478 (2005).
51. Lopez, M. N., Wilding, T. J. & Huettner, J. E. Q/R site interactions with the M3 helix in GluK2 kainate receptor channels revealed by thermodynamic mutant cycles. *J. Gen. Physiol.* **142**, 225–239 (2013).
52. Greger, I. H., Khatri, L., Kong, X. & Ziff, E. B. AMPA receptor tetramerization is mediated by Q/R editing. *Neuron* **40**, 763–774 (2003).
53. Mansour, M., Nagarajan, N., Nehring, R. B., Clements, J. D. & Rosenmund, C. Heteromeric AMPA receptors assemble with a preferred subunit stoichiometry and spatial arrangement. *Neuron* **32**, 841–853 (2001).
54. Greger, I. H., Akamine, P., Khatri, L. & Ziff, E. B. Developmentally regulated, combinatorial RNA processing modulates AMPA receptor biogenesis. *Neuron* **51**, 85–97 (2006).
55. Turetsky, D., Garringer, E. & Patneau, D. K. Stargazin modulates native AMPA receptor functional properties by two distinct mechanisms. *J. Neurosci.* **25**, 7438–7448 (2005).
56. Semenov, A., Moykkynen, T., Coleman, S. K., Korpi, E. R. & Keinänen, K. Autoinactivation of the stargazin-AMPA receptor complex: subunit-dependency and independence from physical dissociation. *PLoS ONE* **7**, e49282 (2012).
57. Cull-Candy, S. G., Howe, J. R. & Ogden, D. C. Noise and single channels activated by excitatory amino acids in rat cerebellar granule neurones. *J. Physiol.* **400**, 189–222 (1988).
58. Shi, S., Hayashi, Y., Esteban, J. A. & Malinow, R. Subunit-specific rules governing AMPA receptor trafficking to synapses in hippocampal pyramidal neurons. *Cell* **105**, 331–343 (2001).
59. Wenthold, R. J., Petralia, R. S., Blahos, J. II & Niedzielski, A. S. Evidence for multiple AMPA receptor complexes in hippocampal CA1/CA2 neurons. *J. Neurosci.* **16**, 1982–1989 (1996).
60. Lu, W. et al. Subunit composition of synaptic AMPA receptors revealed by a single-cell genetic approach. *Neuron* **62**, 254–268 (2009).
61. Zhao, Y., Chen, S., Swensen, A. C., Qian, W. J. & Gouaux, E. Architecture and subunit arrangement of native AMPA receptors elucidated by cryo-EM. *Science* **364**, 355–362 (2019).
62. Rothman, J. S. & Silver, R. A. NeuroMatic: an integrated open-source software toolkit for acquisition, analysis and simulation of electrophysiological data. *Front. Neuroinform.* **12**, 14 (2018).
63. Sigworth, F. J. The variance of sodium current fluctuations at the node of Ranvier. *J. Physiol.* **307**, 97–129 (1980).
64. Wang, J. J., Liu, W. B., Fan, J. & Lu, J. S. Mean activity-coefficients of NaCl in glucose water and sucrose water mixtures at 298.15-K. *J. Chem. Soc. Far Trans.* **90**, 3281–3285 (1994).
65. Colquhoun, D. & Hawkes, A. G. On the stochastic properties of bursts of single ion channel openings and of clusters of bursts. *Philos. Trans. R. Soc. Lond. B Biol. Sci.* **300**, 1–59 (1982).
66. Traynelis, S. F. & Jaramillo, F. Getting the most out of noise in the central nervous system. *Trends Neurosci.* **21**, 137–145 (1998).
67. Winter, G., Lobley, C. M. & Prince, S. M. Decision making in *xia2*. *Acta Crystallogr D Biol. Crystallogr.* **69**, 1260–1273 (2013).
68. Evans, P. R. & Murshudov, G. N. How good are my data and what is the resolution? *Acta Crystallogr D Biol. Crystallogr.* **69**, 1204–1214 (2013).
69. McCoy, A. J. et al. *Phaser* crystallographic software. *J. Appl. Crystallogr.* **40**, 658–674 (2007).
70. Terwilliger, T. C. et al. Iterative model building, structure refinement and density modification with the PHENIX AutoBuild wizard. *Acta Crystallogr. D Biol. Crystallogr.* **64**, 61–69 (2008).
71. Emsley, P., Lohkamp, B., Scott, W. G. & Cowtan, K. Features and development of *Coot*. *Acta Crystallogr. D Biol. Crystallogr.* **66**, 486–501 (2010).
72. Canty, A. & Ripley, B. *boot: Bootstrap R (S-Plus) Functions*. R. package version 1.3-20 (2017).

Acknowledgements

This work was supported by the MRC (MR/J002976/1 to S.G.C.-C. and M.F. and MR/J012998/1 to M.F. and S.G.C.-C.), the Wellcome Trust (086185/Z/08/Z to S.G.C.-C. and M.F.) and the BBSRC (BB/N015274/1 to M.G.G.). M.G.G. is a Wellcome Trust and Royal Society Sir Henry Dale fellow (104194/Z/14/Z). We thank Ingo Greger for providing the GluA2 LBD expression vector, and Trevor Smart, Duncan Laverty, and Ambrose Cole for assistance with crystallography. We thank Mark Mayer for discussion and for comments on an earlier version of the manuscript.

Author Contributions

I.D.C., D.S., T.P.M., M.G.G., M.F. and S.G.C.-C. designed the experiments. I.D.C., D.S. and T.P.M. performed the experiments. I.D.C., D.S., T.P.M., M.G.G., and M.F. analyzed the data. I.D.C., M.G.G., M.F. and S.G.C.-C. interpreted the results. I.D.C. and M.F. prepared the figures. I.D.C., M.F. and S.G.C.-C. wrote the manuscript with input from all authors.

Additional information

Supplementary information accompanies this paper at <https://doi.org/10.1038/s41467-019-12280-9>.

Competing interests: The authors declare no competing interests.

Reprints and permission information is available online at <http://npg.nature.com/reprintsandpermissions/>

Peer review information *Nature Communications* thanks Lonnie P Wollmuth, Wei Lu, and the other, anonymous, reviewer(s) for their contribution to the peer review of this work.

Publisher's note Springer Nature remains neutral with regard to jurisdictional claims in published maps and institutional affiliations.



Open Access This article is licensed under a Creative Commons Attribution 4.0 International License, which permits use, sharing, adaptation, distribution and reproduction in any medium or format, as long as you give appropriate credit to the original author(s) and the source, provide a link to the Creative Commons license, and indicate if changes were made. The images or other third party material in this article are included in the article's Creative Commons license, unless indicated otherwise in a credit line to the material. If material is not included in the article's Creative Commons license and your intended use is not permitted by statutory regulation or exceeds the permitted use, you will need to obtain permission directly from the copyright holder. To view a copy of this license, visit <http://creativecommons.org/licenses/by/4.0/>.

© The Author(s) 2019